Thirumamagal et al., J Powder Metall Min 2017, 6:2
DOI: 10.4172/2168-9806.1000173

Journal of
Powder Metallurgy & Mining

Research Article OMICS International

Comparative Morphological Studies on NiO, CoO and Fe_2O_3 Nanoparticles

Thirumamagal R[1], Irshad Ahamed S[2], Nivetha S[3,4], Saravanakkumar D[1,5], Ayeshamariam A[1,3,4*], Pandiarajan S[5] and Jayachandran M[5]

[1]*Research and Development Centre, Bharathiyar University, Coimbatore, 641046, India*
[2]*Sri Manakula Vinayagar Medical College and Hospital, Kallitheerthalkuppam, Madagadipet, Puducherry, 605107, India*
[3]*Research and Development Center, Bharathidasan University, Thiruchirappalli, 620 024, India*
[4]*Department of Physics, Khadir Mohideen College, Adirampattinam, 614701, India*
[5]*Department of Physics, Devanga Arts College, Aruppukkottai, 626 101, India*

Abstract

Stable oxides of Ni, Fe and Co nanoparticles are synthesized by chemical route using leaf extraction. Structural, biological morphological and magnetic properties were investigated. X ray pattern shows a polycrystalline structure of samples. Diffraction planes of (200), (122) and (200)-oriented crystal structures were revealed by X-ray pattern for NiO, Fe_2O_3 and CoO respectively. Hexagonal, orthorhombic and cubic crystal structures have been revealed respectively for NiO Fe_2O_3 and CoO nanoparticles. Microscopic structure has been detected by using of Scanning Electron Microscopy. Ni, Fe and Co is present at 71%, 78.8%, 79% as indicated by EDS analysis respectively. Mass magnetization values of 51, 61 and 54 emu/g are recorded for NiO, Fe_2O_3 and CoO nanoparticles.

Keywords: Ni; Fe; Co; Metal oxides; High transparency; Magnetic properties

Introduction

The aim of this study was to find out comparative studies of metal oxides of Ni, Fe and Co mediated oxidative stress synthesized NPs. This study suggested that bare CoO NPs are a toxic for primary human immune cells that deals directly with human health. Surface modification or surface functionalization may open the gateway for further use of CoO NPs in different industrial use or in biomedical sciences [1,2]. The highest values of coercive field and saturation magnetization were obtained for the sample at x¼1.0, while the lowest values were obtained in the sample with the highest Co excess (x¼2.5). The results indicated that the used synthesis route was suitable for the synthesis of cobalt ferrite with moderate saturation magnetization and high coercive field values [3-5]. In addition, the de-amination is contributed by the nucleorphilic attack of water molecule to the carbon atom of aromatic ring bonded to NH_2 group. After the de-amination reaction, the intermediate product is phenol. The following de-hydroxyl reaction by FeO domain proceeds immediately. The final product is benzene that is observed in all FIT involved catalytic routes [4]. Nanostructured iron oxides have been widely used in catalysis, adsorption, sensor, biomedicine, and so on. In this study, iron oxide nanoparticles containing nanosized cavities were prepared by hydrothermal treatment of a colloidal dispersion of iron hydroxide. Moreover, the iron oxide nanoparticles calcined 7-15 nm and 5-12 nm-diameter cavities, respectively. These peculiar structures might be conducive for some applications such as adsorption involving large molecules [5]. Pure NiO, CoO and Fe_2O_3 exhibits anti ferromagnetic nature, which transforms into ferromagnetic one with moderate moment at room temperature with decreasing crystallite size. On the other hand, annealing of as-milled powders showed a large reduction in magnetic moment and the rate of decrease of moment strongly depends on the milling conditions. The observed properties are discussed on the basis of crystallite size variation, defect density, oxidation/reduction of Ni, Co and Fe and interaction between un- compensated surfaces and particle core with lattice expansion [6,7].

Experimental Section

Materials used for the synthesis of Nickel oxide nanoparticles are Nickel Chloride salt ($NiCl_2$), cobalt chloride $CoCl_2$ and ferrous chloride $FeCl_2$ the salt was purchased from Merck, were the main sources of producing synthesized NiO, FeO and CoO, these three salt solutions were placed separately in three different beakers. These salt solutions were prepared in 1M ratio, with these individual beakers, 1mM NaOH was added separately 1 µL of coreopsis leaf broth extract with, 30 µL of milli Q water and then boiling the mixture before finally decanting it, freshly prepared double distilled water was used throughout the experimental work, the mixture was heated to 250°C for 20 minutes followed by filtering. Maintain this temperature for the entire reaction. Broth stored in refrigerator at 4°C. Within an hour (50 minutes) cherry red solution was obtained. Different plant extracts require different times to complete the reaction. The extract was added to 3.5×10^{-4} M Nickel chloride aqueous solution, obtaining different samples with different pH (the volumetric ratio mixture extract/Nickel chloride salt control sample containing only Nickel chloride salt. We have synthesized the Nickel oxide, cobalt oxide and ferrous oxide nanoparticles using this plant. The leaves were collected and the leaf broth was prepared by taking 5 g of thoroughly washed and finely cut leaves and 15 µL of milli Q water. Then the leaves were nicely crushed in mortar pestle, transferred the nicely crushed leaves in to centrifuge tube and centrifuged at 10000-11000 rpm for 10 min at 4 to 5°C. 1 µL of nitric acid was mixed with the 1 µL of biological extract and added into 30 µL of boiling milli Q water. Within a few minutes; the solution developed a distinct characteristic colour (Green) and later varied the volume of concentration (50 µL and 100 µL), like that the experiment is repeated for different pH (7, 9) by keeping the volume leaf extract (25 µL) constant with constant stirring till the reaction got over (20 min) and studied the absorption of samples by using spectrophotometer.

***Corresponding author:** Ayeshamariam A, Department of Physics, Khadir Mohideen College, Adirampattinam, 614701, India, Fax: 04373-240810; Tel: 9486738806; E-mail: aismma786@gmail.com

Received June 19, 2017; **Accepted** June 25, 2017; **Published** July 01, 2017

Citation: Thirumamagal R, Irshad Ahamed S, Nivetha S, Saravanakkumar D, Ayeshamariam A, et al. (2017) Comparative Morphological Studies on NiO, CoO and Fe_2O_3 Nanoparticles. J Powder Metall Min 6: 172. doi:10.4172/2168-9806.1000173

Results and Discussion

Structural characterization

The XRD pattern of NiO, CoO and Fe_2O_3 were shown in Figure 1. All the observed diffraction peaks are indexed within face centred cubic (FCC) structure of NiO phase, in agreement with JCPDS card No. 451027 (Hexagonal) and FCC structure of CoO phase in agreement with JCPDS card-711178 (Cubic) and third nanoparticle Fe_2O_3 phase in agreement with JCPDS-897047 Orthorhombic. It can be noticed that the peak are broad, indicating the formation of nanocrystalline NiO, CoO and Fe_2O_3 phase. In addition, with annealing temperature of 250°C, the intensity of peaks increases thereby enhanced crystallinity (Table 1). The crystallite size (D), dislocation density (δ), strain (ε), and lattice parameter (a), were calculated using the following formula:

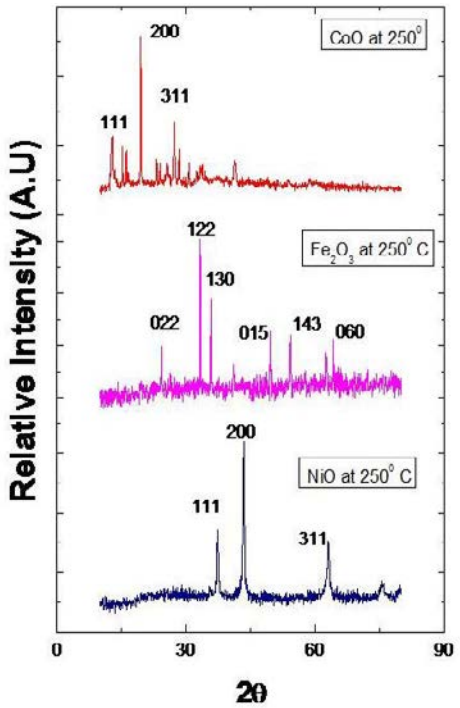

Figure 1: XRD analysis of NiO, CoO and Fe_2O_3 at 250°C.

$$D = \frac{0.9\ \lambda}{\beta\ \cos\theta} \quad (1)$$

Where λ is the wavelength of the x-ray source, β is the full-width at half-maximum (FWHM in radian and θ is the Bragg's angle;

The dislocation parameter is then calculated;

$$\delta = \frac{1}{D^2} \quad (2)$$

The strain is then determined by the following relation,

$$\varepsilon = \frac{\Delta d}{d_o} = \left(\frac{d_{exp} - d_{hkl}}{d_{hkl}}\right) \quad (3)$$

$$a = \frac{\Delta d}{d_o} \quad (4)$$

Where d_{exp} and d_{hkl} represent the experimental and for standard values of interplanar distance respectively calculated values are reported in Table 2. It can be noticed that the value of the crystallite size increases slightly setting in the range 29.82, 26.103 and 31.289 nm, due to grain growth. According to formula (2), the smaller value of the crystallite size, the larger the value of the dislocation density (inversely proportional), which indicates a better crystalline quality. From Table 1, it can be seen that the prepared films exhibit a compressive strain (all values are positive). In addition, when annealing temperature increases, the strain value increases, which is may be associated with the formation of oxygen vacancies [8].

Scanning electron microscopy with EDAX

Morphological studies of microstructure analysis deals with agglomeration of the particles due to biosynthesis of the leaf extract.

Sample	Lattice constant Calculated (Å)			Crystal size size D= $\frac{0.94\lambda}{\beta Cos\theta}$ (nm)	Strain $\frac{\Delta d}{d_o} = \left(\frac{d_{exp} - d_{hkl}}{d_{hkl}}\right)$ × 10^{-3} lines/m^2	JCPDS
NiO	a=2.701	C=4.412		29.823	1.269	JCPDS -451027 Hexagonal $\frac{1}{d^2} = \frac{4}{3}\left[\frac{h^2+hk+k^2}{a^2}\right] + \frac{l^2}{c^2}$ Volume V= $\left(\frac{\sqrt{3a^2C}}{2}\right)$ Strain= $\beta\cos\theta/4$
CoO	a=4.527			26.103	2.912	JCPDS-711178 a=4.263 A⁰ Cubic $d_{hkl} = \frac{a}{\sqrt{h^2+k^2+l^2}}$
Fe_2O_3	a=5.011	b =8.62	C=9.314	31.289	2.011	JCPDS -897047 Orthorhombic a=5.095 b=8.789 c=9.437 $\frac{1}{d^2} = \frac{h^2}{a^2} + \frac{k^2}{b^2} + \frac{l^2}{c^2}$ V= abc

Table 1: Structural analysis of NiO, CoO and Fe_2O_3 Nanoparticles annealed @250°C.

Sample	Lattice constants Calculated (Å)			Crystal size size D=(nm)	Strain (x 10^{-3} lines/m^2)
NiO	a=2.701		c=4.412	29.823	1.269
CoO	a=4.527			26.103	2.912
Fe_2O_3	a=5.011	b=8.62	c=9.314	31.289	2.011

Table 2: Structural and optical analysis of NiO, CoO and Fe_2O_3 Nanoparticle at 250°C.

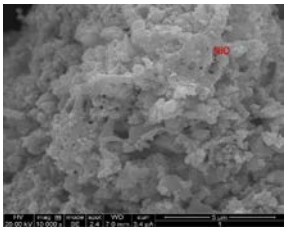

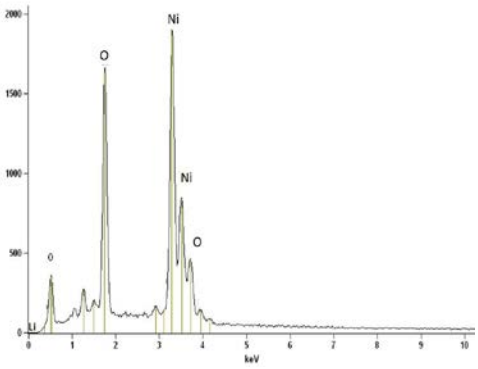

Element	Net Counts	ZAF	Weight %	Atom %	Formula
Ni	0	8.633	0.00	0.00	Ni
O	3220	7.599	34.25	68.64	O
Ni	1116	2.699	1.32	1.74	Ni
O	17263	1.604	13.49	15.40	O
Ni	37509	1.185	50.94	14.23	Ni
Total			100.00	100.00	

Figure 2: (a and b) SEM images and EDAX analysis of NiO NPs at 250°C.

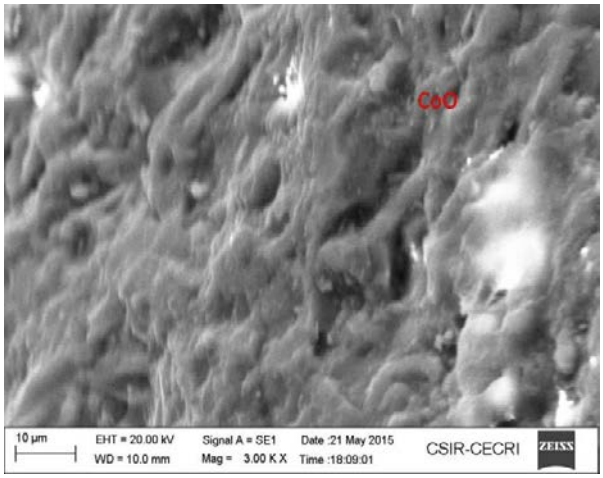

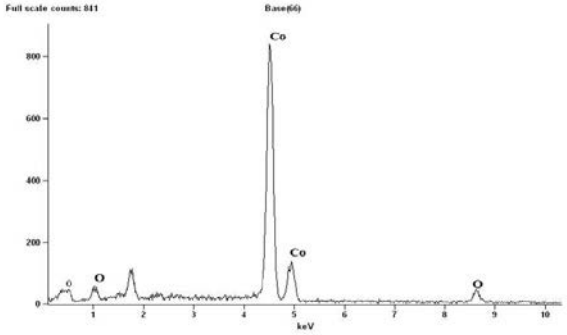

Element Line	Net Counts	Weight %	Atom %	Formula
O K	256	10.19	25.98	O
Co K	13632	79.03	67.30	Co
Co L	290	—	—	
O K	562	10.77	6.72	O
Total		100.00	100.00	

Figure 3: (a and b) SEM images and EDAX analysis of CoO NPs at 250°C.

Coreopsis leaf extract was added in the equal ratio of these three mother solutions of the particles. The as-prepared NPs were annealed at constant temperature of 250°C. The particles distributions of these NPs were almost constant shown in Figures 2a, 2b, 3a, 3b, 4a and 4b respectively. Scanning Electron Microscopy for creating nanofibers of these oxides materials and its elemental analysis confirmed the metal oxides and its presence in its condition (Figures 2-4).

Transmission electron microscopy of NiO, FeO and CoO

Transmission Electron Microscopy confirmed the size distribution of metal oxides NPs which were below 100 nm, shown in Figure 5a-5c. The diffraction planes of x-ray diffractometer were well matched with SAED pattern. This efficient tool exhibits the real morphology of single particles and its agglomerations of the outcomes of the product. Slight dark batches present in these three particles distributions verify the biosynthesized products.

FT-IR analysis

Figure 6 illustrates the complementary information in the presence of NiO, CoO and Fe_2O_3, FT-IR analysis is observed on NiO, CoO and Fe_2O_3 in the spectral region of 400 to 4000 cm^{-1}. The characteristic absorption peaks of oxide groups belong to 1388 cm^{-1}, 1625 cm^{-1}. For the OH^- group of NiO, peak positions are 2388 cm^{-1}. The bending mode of H_2O bond at 1625 cm^{-1} as well as its stretching mode in the range of 3000-3700 cm^{-1}, which is almost overlapped by the O-H vibration mode of NiO, CoO and Fe_2O_3 at 2358 cm^{-1}, are observed in the FT-IR analysis of the Oxide materials [9] (Table 3).

Magnetic studies

The experimental results for NiO, CoO and Fe_2O_3 are more complete and will, therefore, be treated first. Thus, we note first that the magnetization curves for these samples for the present particle size range (i.e. below about 50 nm) and manifest a peak at about 29

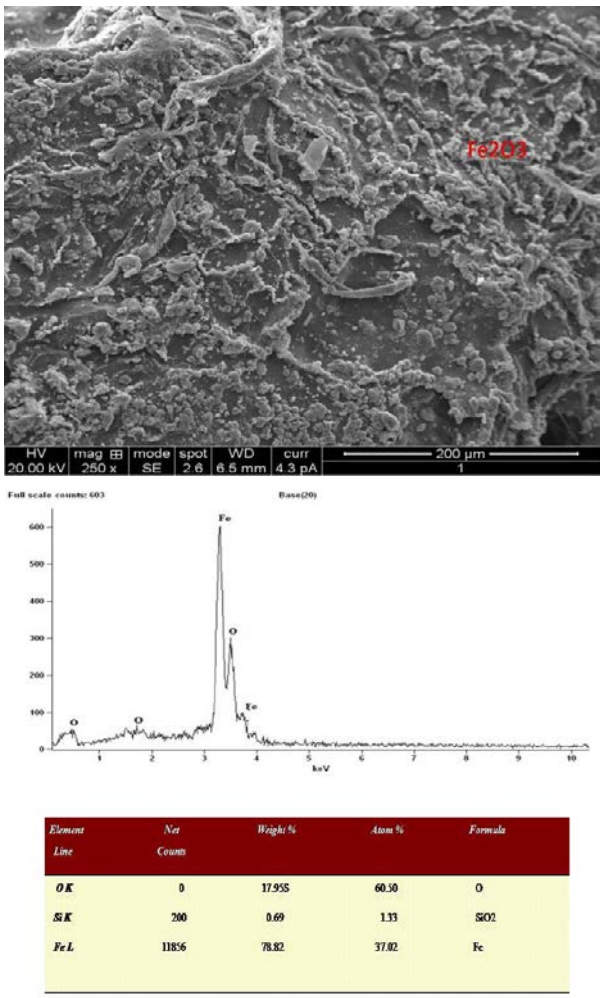

Figure 4: (a and b) EM images and EDAX analysis of Fe_2O_3 NPs at 250°C.

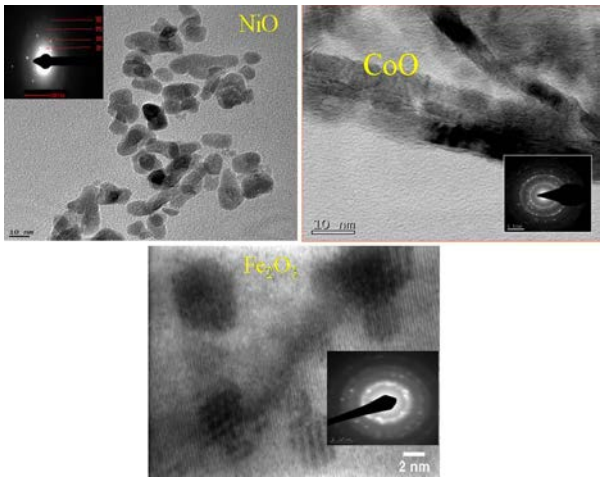

Figure 5: (a-c) TEM and SAED pattern analysis of Fe_2O_3 NPs at 250°C.

K (which should approximate the Néel temperature, known to be a degree or two smaller than the peak temperature and converge at about 100 K (Table 4). The inverse susceptibility shown in Table 4 manifest an anti-ferromagnetic behavior, namely, $\chi_{(T)}=\chi o+C/(T-\theta)$ with a Weiss

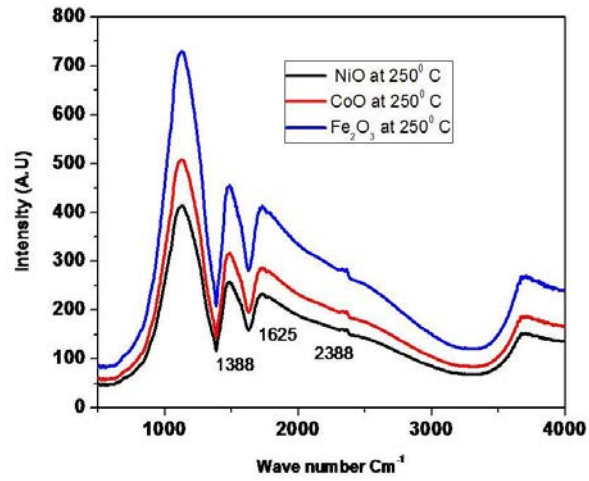

Figure 6: FTIR analysis of NiO, CoO and Fe_2O_3 NPs at 250°C.

	NiO	CoO	Fe_2O_3
Coercivity (Hci) (G)	23.866	25.169	27.160
Magnetization (M_s) (emu/g)	52.505	54.826	61.369
Mass (mg)	1.0000	1.0000	1.0000
Retentivity (M_r) ($\times 10^{-3}$ emu/g)	46.173	47.236	48.325

Table 3: Magnetic calculated parameters of NiO, CoO and Fe_2O_3 nanoparticles annealed at 250°C.

temperature $\theta<0$. Here C is the Curie constant and χ_o comprises an admixture of several contributions, including various magnetic phases contributions a temperature independent orbital contribution and a small diamagnetic contribution measured in this system elsewhere to be approximately 2.06×10^{-6} emu/Oe.g for NiO (i.e. relatively small), 2.53×10^{-6} emu/Oe.g, for CoO and 2.96×10^{-6} emu/Oe.g for Fe_2O_3. Choosing to find the values of Curie constant for the sample Fe_2O_3 neglecting χ_o yields a Curie constant CB≈6.54 10^{-3} K emu/(g Oe), and hence an effective moment per ion μ_{eff}≈3.69 µB, with θB≈−55 K. The determination of θ is, however, known to be problematical and a large range of values is reported in the literature (Figure 7). On the assumption that the overall magnetic behavior m(Ho) (Figure 7) of this nano-particulate system can be expressed as a linear combination of an average antiferromagnetic behavior for the core component and an average superparamagnetic behavior for the shell component it would be given also Chen et al. [10].

Antibacterial activity of compounds against bacterial pathogens using well diffusion method

The antibacterial activities were evaluated against *E. coli*, a Bacillus and Pseudomonas. The bacteria were thawed on ice for 30 minutes before being placed on an agar plate. The plate was then dried before incubation for 17 h in a standard cell culture environment (37°C, 7% CO_2, and 97% air). A single colony of *E. coli* was selected using a 10-µL loop and inoculated into a centrifuge tube containing 5 mM of cryptic soy broth. Bacteria in the centrifuge tube were then incubated at 37°C under agitation at 200 rpm for another 15 h. At that point, the bacteria solution was diluted in cryptic soy broth to an optical density of 0.52 at 600 nm using a microplate reader. According to the standard curve correlating bacteria number with optical density, this value was equivalent to 5×10^6 cells/mL. The cells were further diluted in cryptic soy broth to 5×10^4 cells/mL before being added to a new centrifuge tube at 5 mL/tubes. Concentrated of metal oxides of these three in solution

Microbes	Zone of Inhibition in mm NiO			Zone of Inhibition in mm CoO			Zone of Inhibition in mm Fe_2O_3		
	25 µl	50 µl	100 µl	25 µl	50 µl	100 µl	25 µl	50 µl	100 µl
E. coli	0.8	1.6	1.3	0.8	1.4	1.1	0.7	1.0	1.3
Bacillus	1.1	1.0	1.0	0.9	1.1	1.0	0.8	0.8	0.9
Pseudomonas	0.7	0.9	1.1	0.9	1.0	1.1	0.5	0.5	0.6

Table 4: Antibacterial activity analysis details.

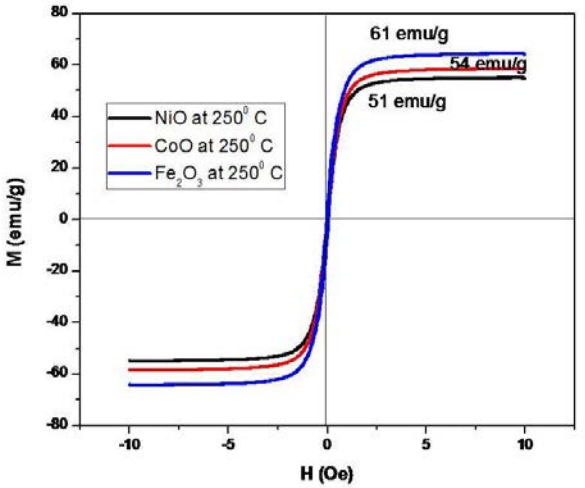

Figure 7: Magnetization profile vs. applied magnetic field of NiO, CoO and Fe_2O_3 nanoparticles annealed at 250°C.

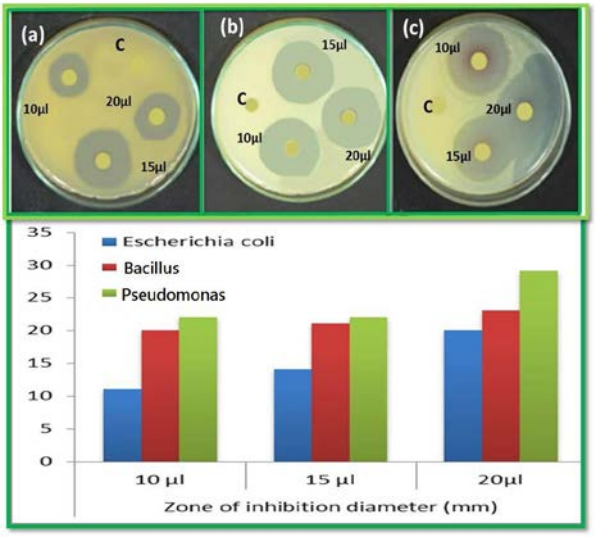

Figure 8: (a-c) Bacterial analysis of NiO, CoO and Fe_2O_3 nanoparticles annealed at 250°C.

were added to bacteria tubes at different doses (2 mM (low dose), 5 mM (medium dose), and 10 mM (high dose)). A tube of bacteria without nanoparticles served as a control. Bacteria were then incubated under agitation for different concentration solution was transferred to a 100-well plate for optical density readings at 600 nm using a microplate reader. The plates were incubated at 30°C for 24 h, and then the diameters of the zone of inhibition were measured in millimetres. Each antibacterial assay was performed in triplicate and mean values were reported (Figure 8). NiO, Fe_2O_3 and CoO were treated for antibacterial activity against *E. coli*, Bacillus and Pseudomonas as shown in the Figure 8a-8c. These species were grown in Luria Bertaniborth (LB) and Tryptic soy Borth (TSB) respectively and incubated at 35°C for all the assays overnight cultures were used in 1:100 dilutions in Muller Hinton agar (MHA) medium. Wells with a diameter of 3 mm were then punched out of the swabbed plates. Dimethyl sulfoxide (DMSO) was served as control. Then, the plates were incubated at 35°C for 36 h. In the zone of inhibition was measured and the results were expressed in millimetre diameter. NiO, Fe_2O_3 and CoO, which is attributed to the medium. The antibacterial results showed that for NiO, Fe_2O_3 and CoO nanocomposite material has some significant effect on the bacterial growth for NiO, Fe_2O_3 and CoO nanocomposites portrayed an excellent acitivity against *S. aureus*, *E. hermannii*, then the *P. vulgarias* reverse case was obtained with 1:100 ratios. In the presence of reactive oxygen species (ROS) generated by for NiO, Fe_2O_3 and CoO nanoparticles are responsible for their bacterial activity. It was further showed that the antibacterial behaviour of for NiO, Fe_2O_3 and CoO nanocomposites could be due to the chemical interactions between hydrogen and membrane proteins, or other chemical species produced in the presence of for NiO, Fe_2O_3 and CoO nanoparticles. It was shown in the study that nano sized for NiO, Fe_2O_3 and CoO nanoparticles are responsible for inhibiting bacterial growth. The photographs of the antimicrobial activity of the NiO, CoO and Fe_2O_3 composites nanoparticles were investigated against *S. aureus* (MTCC 1430) followed by *E. coli* (MTCC 739) by agar diffusion assay and Resazurin Microtitre Assay (REMA) (Sotirious Baskoutas) [11]. Since *Staphylococcus aureus* and the *Escherichia coli* have been implies to be the important common pathogens in biomaterial-associated infections. However, there are some differences between gram positive *S. aureus* and gram negative *E. coli*. *S. aureus* has slightly less bacterial activities in growth curves, protein leakage, and inactivation of LDH (Lactate Dehydrogenase activity) than *E. coli*. The morphological destruction of bacterial cell of *S. aureus* was weak than *E. coli*. This difference was possibly attributable to the difference of the peptidoglycan layer of the bacterial cell between gram positive *S. aureus* and *E. coli*, an essential function of the peptidoglycan layer is to protect against antibacterial agents such as antibiotics, toxins, chemicals, and cell membrane [12-14]. The oxide materials with different samples of NiO, CoO and Fe_2O_3 are important factor for antimicrobial activity. Initially NiO sample, CoO sample and Fe_2O_3 sample, it can be used as an antimicrobial material or coatings in various day to day applications (bath room tiles, doorknobs, packing materials etc.) by controlling the spread of disease causing microbes. Since metal oxides have the good adsorption property and they are well known for its photo-degradation nature the composites can be used as absorbent and degradation agent for the pollutants. Hence the combination for the NiO, CoO and Fe_2O_3 has excellent applications in biomedical, antimicrobial and environmental friendly applications [15,16]. In case NiO highest dipping rate of sample clearly implies that the bacterial growth decreases and exponentially with increasing dipping rate increases the process up to certain concentration. In such a case, basically *E. coli* has a relatively thin cell wall made of peptidoglycans and lipopolysaccharide [17,18]. It is concluded that increasing the dipping rate due to increase the metal oxides change of inhibited area of zone also increases due to change antimicrobial activity of against Bacillus (MTCC 1430) followed by

E. coli (MTCC 739) by agar diffusion assay and Resazurin Microtitre Assay (REMA). The initial concentration of the microorganisms used was 1×10^8 cells/ml (test culture). The agar diffusion assay is performed on Mueller-Hinter (MH) agar. 1% test culture is seeded into the medium before pouring it in to Sterile Petri plates to form a layer of 4 mm thickness. Metal oxides are loaded on sterile discs (Himedia). Which are placed on the MH agar plates and incubated for 24 h at 37°C. The results are recorded by observing the zone of inhibition as shown in Table 4 [19]. It is good agreement with reported that *S. aureus* has exhibited the most susceptibility to the composites in comparison with *E. coli* [20]. The addition of the outer membrane of the gram-negative bacteria cells influences the permeability of many molecules. Under certain conditions, the gram-negative bacteria are more resistant to many chemical agents than gram-positive cells [21]. The antibacterial activity of the Bacillus spp composites on *E. coli*. The samples were tested for antimicrobial activity by Disc Diffusion Method against pathogenic organisms such as *E. coli* and Bacillus spp. The pure cultures of organisms were sub-cultured on nutrient broth at 35°C on a rotary shaker at 300 rpm. Loop full isolated subculture swabbed on MHA agar plate. The pre culture plate was prepared by standard method [22-24]. After solidification of the agar plate, different types of test pathogens were swabbed in each of the agar plate using sterile cotton buds and labeled clearly. The plates were then supplemented with different composite thin films and incubated at 37°C for 24 h of incubation to observe the zone of inhibition.

Conclusion

NiO, Fe_2O_3 and CoO were successfully synthesised by biosynthesis method. The effect of annealing temperatures at 250°C on their comparative structural and morphological properties of metal oxides was investigated using X-ray diffraction and Scanning Electron Microscopy and Transmission Electron Microscopy respectively. In addition, the characterizations, analysis and simulation studies recommended these three unstable metal oxides were very much helpful for magnetic and biological applications.

References

1. Hakim A, Hossain J, Khan KA (2009) Temperature effect on the electrical properties of undopedNiO thin films. Renew.Energy 34: 2625-2629.
2. Zhi-Guo Y, Li-Ping Z, Yan-Min G, Zhi-Zhen Y, Bing-Hui Z (2011) Preparation and band-gap modulation in MgxNi1-xO thin films as a function of Mg contents. Thin solid Films 519: 5174-5177.
3. Hotovy I, Huran J, Spiess L, Capkovic R, Hascik S (2007) Preparation and characterization of NiO thin films for gas sensor applications. Vacuum 58: 300-307.
4. Van Elp J, Eskes H, Kuiperr P, Sawatzky GA (1992) Electronic structure of Li-doped NiO. Phys Rev B 45: 1612-1622.
5. Kamal H, Elmaghraby EK, Ali SS, Abdel-Hady K (2005) The electrochromicbehavior of Nickel oxide films sprayed at different preparative conditions. Thin Solid Films 483: 330-339.
6. Patil UM, Salunkhe RR, Gurav KV, Lokhande CD (2008) Chemically deposited nanocrystalline NiO thin films for super capacitor application. Appl Surf Sci 255: 2603-2607.
7. Gokul B, Saravanan P, Vinod VTP, MiroslavCernik, Sathyamoorthy R (2015) Synthesis of Ni/NiO nanocomposites by hydrothermal-assisted polyol process and their magnetic properties as a function of annealing temperature. Powder technology 274: 98-104
8. Ayeshamariam A, Kashif M, Arokiaraj S, Bououdina M, Sankaracharyulu MGV (2014) Bio-Synthesis of NiO and Ni Nanoparticles and their characterization. Digest Journal of Nanomaterials and Bio structures 9: 1007-1019
9. Isadafnaz M, Qadir I, Ali M, Janbaz KH (2012) Nanotecnology for Imaging and Drug Delivery in Cancer. J Chem Soc Pak 34.
10. Chen CJ, Liao CH, Hsu KC, Wu YT, Wu JC (2011) P-N junction mechanism on improved NiO/TiO_2 photocatalyst. Catalysis communications 12: 1307-1310.
11. Baskoutas S, Terzis AF (2006) Size dependent band gap of colloidal quantum dots, American institute of physics. J appl Phys 99: 013708.
12. Hill AW, Shears AL, Hibbitt KG (1976) Increased antibacterial activity against Escherichia Coli in Bovine serum after the induction of endotoxin tolerance. American society for microbial 14: 257-265.
13. Nathanael AJ, Mangalaraj D, Chen PC, Ponpandian N (2010) Mechanical and photocatalytic properties of hydroxyapatite/titania nanocomposites prepared by combined high gravity and hydrothermal process. Comp Sci Tech 70: 419-26.
14. Soo-Hwan K, Seonlee H, Ryu D, Choi S (2011) Antibacterial activity of silver-nanoparticles against staphylococcus aureus and Escherichia Coli. Korean J Microbial Biotechnol 39: 77-85.
15. Zhang HT, Ding J, Chow GM (2009) Synthesis and characterizations of Ni-Fe@ spinel oxide core–shell nanoparticles. Materials Research Bulletin 44: 1195-1199.
16. Raposo M, Ferreira Q, Ribeiro PA (2007) A guide for atomic force microscopy analysis of soft-condensed matter. Modern research and educational topics in microscopy 1: 758-769.
17. Lee HU, Jeong YS, Park SY, Jeong SY, Kim HG (2009) Surface properties and cell response of fluoridated hydroxyapatite/TiO_2 coated on Ti substrate. Current Appl Phys 9: 528-533.
18. Satyajit D, Sarker, Nahar L, Kumarasamy Y (2007) Microtitre plate based antibacterial assay incorporating resazurin as an indicator of cell growth, and its application in the in vitro antibacterial screening of phytochemicals. Methods 42: 321-324.
19. Naz N, Iqbal MZ (2011) Synthesis, Spectroscopic and Biological Studies of Transition Metal Complexes of Novel Schiff Bases Derived from Cephradine and Sugars. Science International (Lahore) 23: 27-31.
20. Nathanael AJ, Lee JH, Mangalaraj D, Hong SI, Rhee YH (2012) Multifunctional properties of hydroxyapatite/titania bio-nano-composites: bioactivity and antimicrobial studies. Powder Technology 228: 410-415.
21. Chen, Da-Peng (2012) Growth mechanism and magnetic properties of highly crystalline NiO nanocubes and nanorods fabricated by evaporation. Crystal Growth & Design 12: 2842-2849.
22. Arunpandian B (2015) Biomaterials based nano-applications of Aloe vera and its perspective: a review. RSC Advances 5: 86199-86213.
23. Helan V, Prince JJ, Al-Dhabi NA, Arasu MV, Ayeshamariam A, et al. (2016) Neem leaves mediated preparation of NiO nanoparticles and its magnetization, coercivity and antibacterial analysis. Results in Physics 6: 712-718.
24. Ayeshamariam A, Sankaracharyulu GV, Kashif M, Hussain S, Bououdina M, et al. (2015) Antibacterial Activity Studies of Ni and SnO_2 loaded Chitosan Beads. Materials Science Forum 832: 110-122.

Citation: Thirumamagal R, Irshad Ahamed S, Nivetha S, Saravanakkumar D, Ayeshamariam A, et al. (2017) Comparative Morphological Studies on NiO, CoO and Fe_2O_3 Nanoparticles. J Powder Metall Min 6: 172. doi:10.4172/2168-9806.1000173